GPR Without a Source: Cross-Correlation and Cross-Convolution Methods

Evert Slob and Kees Wapenaar

Abstract—Several formulations exist for retrieving the Green's function from cross correlation of (passive) recordings at two locations. For media without losses, these known formulations retrieve Green's functions from sources on a closed boundary. Until recent, these formulations were only developed for acoustic waves in fluids and elastodynamic waves in solids. Now, Green's function representations for electromagnetic (EM) waves in matter exist and can be exploited for passive ground-penetrating radar (GPR) applications using transient or ambient noise sources, either natural or man-made. We derive general exact EM Green's function retrieval formulations based on cross correlations and cross convolutions of recorded wave fields. For practical applications, simplified forms are derived that directly apply to field recordings due to unknown uncorrelated noise or transient sources. Only naturally present sources are needed, which allows for all kinds of applications of "GPR without a source." We illustrate the consequences of using the simplified forms for Green's function retrieval with 2-D numerical examples. We show that in dissipative media, the Green's function is most accurately retrieved using the cross-convolution method when the sources are located on a sufficiently irregular boundary.

Index Terms—Green function, interferometry, radar, radiometry.

I. Introduction

SINCE the early theoretical work of Clearbout [3], and the experimental work of Weaver and Lobkis [12], [32], many others have contributed to our understanding of Green's function retrieval from cross correlating two recordings in a noise field [2], [6], [15], [17], [22], [26], [27], [29], [33]. From 1-D and pulse-echo experiments, the subject has evolved to arbitrary 3-D media, ranging from having statistical properties to being fully deterministic.

Recently, representations have been derived for electromagnetic (EM) waves and fields in lossless media, using transient or uncorrelated noise sources [18], [19]. Here, we derive representations of EM Green's functions for nonconductive media and for conductive media. When the sources lie on a closed boundary, cross-correlation-type techniques cannot be used for recordings of wave phenomena where a substantial part of the wave energy is converted into heat or for diffusive fields. Under certain conditions and with sources distributed in a finite volume it can be used for recordings of diffusive fields [23]. Here, we investigate sources located on the boundary of a finite

domain. The formulations derived here can be used with active sources, but also work with natural noise or transient sources, which opens up all kinds of applications of "GPR without a source." For GPR applied to shallow subsurface investigations, some energy is always converted into heat. We show that if the energy loss factor is not high the kinematics of the Green's function are recovered correctly. When the loss factor increases near the boundary sources some artifacts can occur in the form of spurious time-symmetric events, although the kinematics of all desired arrivals are correct. For EM waves in conductive media, wave energy is dissipated, while for diffusive EM fields and stationary currents, the wave energy is zero. We show here that for these types of applications exact Green's function representations can be obtained, using sources on the boundary, by convolving two recordings at two different locations using the reciprocity theorem of the time-convolution type. We illustrate the effects of the simplifying assumptions with numerical examples.

II. Causal and Time-Reversed Causal Equations

All representations that are derived in this paper are valid in the time domain for transient or noise signals, but we develop our theory in the frequency domain. To this end, we define the time-Fourier transform of a space-time-dependent vector-quantity as

$$\hat{\boldsymbol{u}}(\boldsymbol{x}, \omega) = \int\limits_{t=0}^{\infty} \exp(-j\omega t)\boldsymbol{u}(\boldsymbol{x}, t)dt \qquad (1)$$

where j is the imaginary unit and ω denotes angular frequency.

In the space-frequency domain, Maxwell's equations in matter are given in matrix-vector form [30] by

$$\boldsymbol{D}_x\hat{\boldsymbol{u}} + [\hat{\boldsymbol{B}} + j\omega\boldsymbol{A}]\hat{\boldsymbol{u}} = \hat{\boldsymbol{s}} \qquad (2)$$

where the field vector $\hat{\boldsymbol{u}}$ is given by $\hat{\boldsymbol{u}}^{\mathrm{T}}(\boldsymbol{x}, \omega) = (\hat{\boldsymbol{E}}^{\mathrm{T}}, \hat{\boldsymbol{H}}^{\mathrm{T}})$, $\hat{\boldsymbol{E}}$ and $\hat{\boldsymbol{H}}$ being the electric and magnetic field vectors and the superscript T denoting transposition, $\hat{\boldsymbol{s}}^{\mathrm{T}}(\boldsymbol{x}, \omega) = -(\{\hat{\boldsymbol{J}}^e\}^{\mathrm{T}}, \{\hat{\boldsymbol{J}}^m\}^{\mathrm{T}})$ is the source vector, with $\hat{\boldsymbol{J}}^e$ and $\hat{\boldsymbol{J}}^m$ the external electric and magnetic current density vectors, while $\boldsymbol{D}_x$ is the matrix of spatial differential operators given by

$$\boldsymbol{D}_x = \begin{pmatrix} \boldsymbol{O} & \boldsymbol{D}_0^{\mathrm{T}} \\ \boldsymbol{D}_0 & \boldsymbol{O} \end{pmatrix} \qquad \boldsymbol{D}_0 = \begin{pmatrix} 0 & -\partial_3 & \partial_2 \\ \partial_3 & 0 & -\partial_1 \\ -\partial_2 & \partial_1 & 0 \end{pmatrix}. \qquad (3)$$

The material matrices are defined as $\boldsymbol{A} = \text{blockdiag}(\boldsymbol{\varepsilon}, \boldsymbol{\mu})$, with $\boldsymbol{\varepsilon}$ and $\boldsymbol{\mu}$ the electric permittivity and magnetic permeability tensors and $\hat{\boldsymbol{B}} = \text{blockdiag}(\hat{\boldsymbol{\sigma}}^e, \hat{\boldsymbol{\sigma}}^m)$, with $\hat{\boldsymbol{\sigma}}^e$ and $\hat{\boldsymbol{\sigma}}^m$ the electric and magnetic conductivity tensors. Notice that we have defined the electric permittivity and magnetic permeability as frequency-independent functions. This presents no loss of generality because all possible relaxation mechanisms are incorporated in the frequency-dependent conductivity tensors. Further, a real-valued diagonal matrix $\boldsymbol{K} = \boldsymbol{K}^{-1}$ is introduced as $\boldsymbol{K} = \text{diag}(-1, -1, -1, 1, 1, 1)$, such that $\boldsymbol{K}\boldsymbol{D}_x\boldsymbol{K} = -\boldsymbol{D}_x = -\boldsymbol{D}_x^{\mathrm{T}}$, $\boldsymbol{K}\boldsymbol{A}\boldsymbol{K} = \boldsymbol{A} = \boldsymbol{A}^{\mathrm{T}}$ and $\boldsymbol{K}\hat{\boldsymbol{B}}\boldsymbol{K} = \hat{\boldsymbol{B}}^{\mathrm{T}}$, where the latter two definitions represent the nonnegative definiteness of the material tensors. Such media are called self-adjoint or reciprocal [5].

For the time-correlation-type reciprocity theorem, we need the time-reversed causal Maxwell's equations, which in the frequency domain is equivalent to taking the complex conjugate Maxwell's equations

$$\boldsymbol{D}_x\hat{\boldsymbol{u}}^* + [\hat{\boldsymbol{B}}^* - j\omega\boldsymbol{A}]\hat{\boldsymbol{u}}^* = \hat{\boldsymbol{s}}^* \qquad (4)$$

where the asterisk denotes complex conjugation.

In the next section, we use the causal fields in the time-convolution-type reciprocity relations and the causal and time-reversed causal fields in the time-correlation-type reciprocity relations. A reciprocity theorem in general interrelates two independent states, labeled A and B, in one and the same domain, but the fields, sources and the medium parameters in the two states need not be the same [1], [5], [11], [16]. In our derivations here, we assume all medium parameters to be the same in both states ($\boldsymbol{A}_A = \boldsymbol{A}_B = \boldsymbol{A}$ and $\hat{\boldsymbol{B}}_A = \hat{\boldsymbol{B}}_B = \hat{\boldsymbol{B}}$).

III. CORRELATION-TYPE REPRESENTATIONS

We start with the global form of the reciprocity theorem of the time-correlation type [1] for the situation applied to the domain $\mathbb{D}$ with closed boundary $\partial\mathbb{D}$, which has a unique outward pointing unit normal $\boldsymbol{n}$. The interaction quantity to consider is given by

$$\hat{\boldsymbol{u}}_A^\dagger\boldsymbol{D}_x\hat{\boldsymbol{u}}_B + \left(\hat{\boldsymbol{u}}_B^{\mathrm{T}}\boldsymbol{D}_x\hat{\boldsymbol{u}}_A^*\right)^{\mathrm{T}} \qquad (5)$$

where the superscript $\dagger$ means complex conjugation and transposition. The heterogeneities are not restricted to occur only inside the domain $\mathbb{D}$, but may extend over all space. Substituting (2) and (4) in this interaction quantity, integrating the result over the domain $\mathbb{D}$ and applying Gauss' divergence theorem to the interaction quantity, yields the global reciprocity theorem of the time-correlation type, given by [30]

$$\int_{\mathbb{D}} \left[\hat{\boldsymbol{u}}_A^\dagger\hat{\boldsymbol{s}}_B + \hat{\boldsymbol{s}}_A^\dagger\hat{\boldsymbol{u}}_B\right] d^3\boldsymbol{x}$$

$$= \oint_{\partial\mathbb{D}} \hat{\boldsymbol{u}}_A^\dagger\boldsymbol{N}_x\hat{\boldsymbol{u}}_B d^2\boldsymbol{x} + \int_{\mathbb{D}} \hat{\boldsymbol{u}}_A^\dagger(\hat{\boldsymbol{B}}^\dagger + \hat{\boldsymbol{B}})\hat{\boldsymbol{u}}_B d^3\boldsymbol{x} \qquad (6)$$

where $\boldsymbol{A}$ does not occur in the equation because we have taken it real-valued and $\boldsymbol{N}_x$ is defined similar to $\boldsymbol{D}_x$, but with ∂_i re-

placed by n_i, $i = 1, 2, 3$ and hence $\boldsymbol{K}\boldsymbol{N}_x\boldsymbol{K} = -\boldsymbol{N}_x = -\boldsymbol{N}_x^{\mathrm{T}}$. Equation (6) is the global reciprocity theorem of the time-correlation type as only products of quantities and complex conjugate quantities occur, which corresponds to correlations of these quantities in the time domain. For a more detailed discussion on reciprocity relations, see de Hoop [5]. Various choices of the sources in the two states lead to exact expressions for the Green's function in terms of cross correlations of observed electric wavefields at the observation points $\boldsymbol{x}_A$ and $\boldsymbol{x}_B$ due to sources on the closed boundary surface $\partial\mathbb{D}$.

To localize the electric field receiver locations at $\boldsymbol{x}_A$ and $\boldsymbol{x}_B$, we specify the artificial point sources by replacing the space- and frequency-dependent 6×1 vector $\hat{\boldsymbol{s}}_A$ by the 6×6 matrix $\boldsymbol{I}\delta(\boldsymbol{x} - \boldsymbol{x}_A)$, $\boldsymbol{I}$ being the identity matrix. The corresponding 6×1 field vector $\hat{\boldsymbol{u}}_A$ is replaced by the 6×6 Green's matrix $\hat{\boldsymbol{G}}(\boldsymbol{x}, \boldsymbol{x}_A, \omega)$, given by

$$\hat{\boldsymbol{G}}(\boldsymbol{x}, \boldsymbol{x}_A, \omega) = \begin{pmatrix} \hat{\boldsymbol{G}}^{Ee} & \hat{\boldsymbol{G}}^{Em} \\ \hat{\boldsymbol{G}}^{He} & \hat{\boldsymbol{G}}^{Hm} \end{pmatrix} (\boldsymbol{x}, \boldsymbol{x}_A, \omega) \qquad (7)$$

where the superscripts $\{E, H\}$ denote the observed field type at $\boldsymbol{x}$ and the superscripts $\{e, m\}$ denote the source type at $\boldsymbol{x}_A$. In the submatrices, each Green's tensor denotes one 3×3 Green's tensor. Each column of $\hat{\boldsymbol{G}}$ represents a field vector at $\boldsymbol{x}$ due one particular source type and component at $\boldsymbol{x}_A$. For state B, we make similar choices, replacing $\hat{\boldsymbol{s}}_B$ by $\boldsymbol{I}\delta(\boldsymbol{x} - \boldsymbol{x}_B)$ and $\hat{\boldsymbol{u}}_B$ by $\hat{\boldsymbol{G}}(\boldsymbol{x}, \boldsymbol{x}_B, \omega)$. From source–receiver reciprocity, we know that [30]

$$\boldsymbol{K}\hat{\boldsymbol{G}}^{\mathrm{T}}(\boldsymbol{x}_B, \boldsymbol{x}_A, \omega)\boldsymbol{K} = \hat{\boldsymbol{G}}(\boldsymbol{x}_A, \boldsymbol{x}_B, \omega). \qquad (8)$$

Depending on the choices for the receiver locations, $\boldsymbol{x}_A$ and $\boldsymbol{x}_B$, being inside or outside $\mathbb{D}$, different Green's function representations are obtained. Using $\boldsymbol{N}_x$ together with (8) in (6) and transposing both sides of the result yields

$$\hat{\boldsymbol{G}}(\boldsymbol{x}_B, \boldsymbol{x}_A, \omega)\chi_{\mathbb{D}}(\boldsymbol{x}_A) + \hat{\boldsymbol{G}}^\dagger(\boldsymbol{x}_A, \boldsymbol{x}_B, \omega)\chi_{\mathbb{D}}(\boldsymbol{x}_B)$$

$$= -\oint_{\partial\mathbb{D}} \hat{\boldsymbol{G}}(\boldsymbol{x}_B, \boldsymbol{x}, \omega)\boldsymbol{N}_x\hat{\boldsymbol{G}}^\dagger(\boldsymbol{x}_A, \boldsymbol{x}, \omega)d^2\boldsymbol{x}$$

$$+ \int_{\mathbb{D}} \hat{\boldsymbol{G}}(\boldsymbol{x}_B, \boldsymbol{x}, \omega)(\hat{\boldsymbol{B}}^\dagger + \hat{\boldsymbol{B}})\hat{\boldsymbol{G}}^\dagger(\boldsymbol{x}_A, \boldsymbol{x}, \omega)d^3\boldsymbol{x} \qquad (9)$$

where $\chi_{\mathbb{D}}(\boldsymbol{x}_A) = \{0, 1/2, 1\}$ for $\boldsymbol{x}_A \in \mathbb{D}'$, $\boldsymbol{x}_A \in \partial\mathbb{D}$, $\boldsymbol{x}_A \in \mathbb{D}\}$ denotes the characteristic set of the domain $\mathbb{D}$ and $\mathbb{D}'$ denotes the complement of $\mathbb{D}$ and $\partial\mathbb{D}$. Equation (9) is a general frequency-domain representation of the EM Green's matrix between $\boldsymbol{x}_A$ and $\boldsymbol{x}_B$ in terms of cross correlations in the time domain of observed electric and magnetic fields at $\boldsymbol{x}_A$ and $\boldsymbol{x}_B$ due to electric and magnetic sources at $\boldsymbol{x}$ on the boundary $\partial\mathbb{D}$ and inside the domain $\mathbb{D}$. To arrive at this representation for the Green's functions, no assumptions have been made on the heterogeneity and relaxation mechanisms inside and outside the domain $\mathbb{D}$. Cross correlations in the time domain are in the frequency-domain multiplications of a function with the complex conjugate of another function, which implies that the phases of the two functions are subtracted from each other.

The Green's function in the left-hand side of (9) can be retrieved since it is a causal function and it does not overlap with the time-reversed causal Green's function, except possibly at $t = 0$.

Assuming the medium losses inside $\mathbb{D}$ are negligible, the second integral in the right-hand side of (9) can be neglected and the resulting equation is suitable to compute the Green's functions from a point source in $\boldsymbol{x}_B$ to a point receiver in $\boldsymbol{x}_A$ by correlating precomputed or measured Green's functions from source points, at $\boldsymbol{x}$, on the closed surface to the points $\boldsymbol{x}_A$ and $\boldsymbol{x}_B$. In view of the symmetry relation of (8) not the whole Green's matrix needs to be computed or measured. An example how this can lead to efficient modeling schemes can be found in [24] and [25], who used the acoustic and elastodynamic equivalents of (9) for computing acoustic and elastodynamic Green's functions of arbitrarily heterogeneous media. In Section VI, we show how (9) can be used in a measurement situation.

Since correlation-type representations, employing sources on $\partial \mathbb{D}$ only, rely on the absence of wave energy dissipation inside $\mathbb{D}$, we also use representations based on the convolution-type reciprocity relation.

IV. CONVOLUTION-TYPE EM GREEN'S FUNCTION REPRESENTATIONS

To allow for dissipative media inside and outside $\mathbb{D}$, and hence nonzero electric and magnetic conduction currents, we now consider the reciprocity theorem of the time-convolution type. We use the interaction quantity

$$\hat{\boldsymbol{u}}_A^{\mathrm{T}} \boldsymbol{K} \boldsymbol{D}_x \hat{\boldsymbol{u}}_B - \left(\hat{\boldsymbol{u}}_B^{\mathrm{T}} \boldsymbol{K} \boldsymbol{D}_x \hat{\boldsymbol{u}}_A\right)^{\mathrm{T}}. \quad (10)$$

Substituting (2) for the two states in this interaction quantity, integrating the result over the domain $\mathbb{D}$ and applying Gauss' divergence theorem to the interaction quantity, we find the global form of the reciprocity theorem of time-convolution type as [30]

$$\int_{\mathbb{D}} \left[\hat{\boldsymbol{u}}_A^{\mathrm{T}} \boldsymbol{K} \hat{\boldsymbol{s}}_B - \hat{\boldsymbol{s}}_A^{\mathrm{T}} \boldsymbol{K} \hat{\boldsymbol{u}}_B\right] d^3\boldsymbol{x} = \oint_{\partial \mathbb{D}} \hat{\boldsymbol{u}}_A^{\mathrm{T}} \boldsymbol{K} \boldsymbol{N}_x \hat{\boldsymbol{u}}_B d^2\boldsymbol{x} \quad (11)$$

where the minus sign in the left-hand side arises because use has been made of $\boldsymbol{D}_x^{\mathrm{T}} \boldsymbol{K} = -\boldsymbol{K} \boldsymbol{D}_x$. Notice that in the convolution-type representations, the relaxation and loss mechanisms do not occur in the expression for reciprocal media and hence, we do not have to assume that the medium is lossless. This is a strong advantage of the convolution-type representations over those of the correlation type.

Making the same replacements as in the previous section, for sources and fields (11) is replaced by

$$\hat{\boldsymbol{G}}(\boldsymbol{x}_B, \boldsymbol{x}_A, \omega) \left[\chi_{\mathbb{D}}(\boldsymbol{x}_A) - \chi_{\mathbb{D}}(\boldsymbol{x}_B)\right]$$
$$= \oint_{\partial \mathbb{D}} \hat{\boldsymbol{G}}(\boldsymbol{x}_B, \boldsymbol{x}, \omega) \boldsymbol{N}_x \boldsymbol{K} \hat{\boldsymbol{G}}(\boldsymbol{x}_A, \boldsymbol{x}, \omega) \boldsymbol{K} d^2\boldsymbol{x}. \quad (12)$$

In case both source locations are outside $\mathbb{D} \cup \partial \mathbb{D}$ or inside $\mathbb{D}$, the boundary integral vanishes [1]. Equation (12) is an exact frequency-domain representation for the EM Green's function between $\boldsymbol{x}_A$ and $\boldsymbol{x}_B$ in terms of cross convolutions in the time domain of impulsive field responses observed at the observation points $\boldsymbol{x}_A$ and $\boldsymbol{x}_B$ due to tangential electric and magnetic point sources, at $\boldsymbol{x}$, on the boundary $\partial \mathbb{D}$ and integrating over all source locations on the closed boundary surface $\partial \mathbb{D}$. Cross convolutions in the time domain are in the frequency-domain multiplications of two different functions, which implies that their phases are added.

All representations that we derive here based on the convolution-type reciprocity theorem are in principle valid for wavefields, diffusion fields, potential fields and flow fields, all fields considered linear. An example of a unified cross-correlation-type interferometric representation can be found in [31], and (12) can be seen as the unified cross-convolution-type interferometric representation.

We call (9) and (12) interferometric representations of EM Green's functions. The process of cross correlation and integration is named interferometry, borrowed from radio astronomy, where it refers to correlation methods applied to radio signals from distant objects and it is similar to the method described in [4]. Applications will be investigated in the next section.

V. MODIFICATIONS FOR EM INTERFEROMETRY

In their present form, (9) and (12) contain matrices $\boldsymbol{N}_x$ and $\boldsymbol{N}_x \boldsymbol{K}$ in the cross-correlation and cross-convolution expressions in the surface integral. For a direct application in terms of correlations and convolutions of observed wave fields due to uncontrolled sources the matrices $\boldsymbol{N}_x$ and $\boldsymbol{N}_x \boldsymbol{K}$ should be diagonalized, in which process a source decomposition is necessary into sources for inward and outward traveling waves and fields. This requires the presence of electric and magnetic current-type sources, which implies they should be available at all positions on the boundary. We first diagonalize the representations by rewriting them in terms of electric field observations only and such that only electric current sources are required on the boundary. In a second step, we make simplifying assumptions for the inward and outward traveling waves. These are necessary for practical transient and uncorrelated noise sources.

A. Correlation-Type Interferometry

Now, we reduce the field vector to the electric field and reduce the full Green's matrix to the electric field Green's tensor for an electric source. Then, we find [21]

$$\hat{\boldsymbol{G}}^{Ee}(\boldsymbol{x}_B, \boldsymbol{x}_A, \omega)\chi_{\mathbb{D}}(\boldsymbol{x}_A) + \left\{\hat{\boldsymbol{G}}^{Ee}(\boldsymbol{x}_B, \boldsymbol{x}_A, \omega)\right\}^* \chi_{\mathbb{D}}(\boldsymbol{x}_B)$$
$$= -\frac{1}{j\omega\mu} \oint_{\partial \mathbb{D}} \hat{\boldsymbol{G}}^{Ee}(\boldsymbol{x}_B, \boldsymbol{x}, \omega)\left\{(\boldsymbol{n} \cdot \nabla)\hat{\boldsymbol{G}}^{Ee}(\boldsymbol{x}_A, \boldsymbol{x}, \omega)\right\}^{\dagger} d^2\boldsymbol{x}$$
$$+ \frac{1}{j\omega\mu} \oint_{\partial \mathbb{D}} \left\{(\boldsymbol{n} \cdot \nabla)\hat{\boldsymbol{G}}^{Ee}(\boldsymbol{x}_B, \boldsymbol{x}, \omega)\right\}\left\{\hat{\boldsymbol{G}}^{Ee}(\boldsymbol{x}_A, \boldsymbol{x}, \omega)\right\}^{\dagger} d^2\boldsymbol{x}.$$
$$(13)$$

To arrive at this simplified expression, with a scalar operator acting on the Green's tensors, it has been assumed that the medium in the neighborhood of the surface is homogeneous and isotropic. The derivative acts on the source coordinate and can be regarded as part of the source. This implies that electric dipoles and quadrupoles are necessary to construct new Green's functions. The presence of dipoles and quadrupoles on the boundary is not likely and hence (13) is not practical. By also assuming that outside the domain $\mathbb{D}$, the medium is homogeneous and isotropic and in addition that the boundary surface is convex, seen from inside $\mathbb{D}$, then outward traveling waves never enter the domain. We assume far-field conditions apply to reduce the differential operator to an algebraic factor [5] and find

$$(\boldsymbol{n} \cdot \nabla)\hat{\boldsymbol{G}}^{Ee}(\boldsymbol{x}_{A,B}, \boldsymbol{x}, \omega) \approx -\frac{j\omega}{c}\hat{\boldsymbol{G}}^{Ee}(\boldsymbol{x}_{A,B}, \boldsymbol{x}, \omega) \quad (14)$$

where inward traveling waves are taken because they contribute to the desired result, while in case both $\boldsymbol{x}_A$ and $\boldsymbol{x}_B$ are located inside $\mathbb{D}$, only inward traveling waves are recorded. The amplitude factor is correct for waves leaving the boundary in the opposite direction of the unit normal. Substituting the result of (14) into (13) yields

$$\hat{\boldsymbol{G}}^{Ee}(\boldsymbol{x}_B, \boldsymbol{x}_A, \omega)\chi_{\mathbb{D}}(\boldsymbol{x}_A) + \left\{\hat{\boldsymbol{G}}^{Ee}(\boldsymbol{x}_B, \boldsymbol{x}_A, \omega)\right\}^* \chi_{\mathbb{D}}(\boldsymbol{x}_B)$$
$$= -\frac{2}{c\mu}\oint_{\partial\mathbb{D}} \hat{\boldsymbol{G}}^{Ee}(\boldsymbol{x}_B, \boldsymbol{x}, \omega)\left\{\hat{\boldsymbol{G}}^{Ee}(\boldsymbol{x}_A, \boldsymbol{x}, \omega)\right\}^\dagger d^2\boldsymbol{x} + \text{``ghost''}$$

$$(15)$$

where "ghost" refers to spurious events due to cross products of inward and outward propagating waves that arise in the situation when either $\boldsymbol{x}_A$ or $\boldsymbol{x}_B$ is outside $\mathbb{D}$, from the assumption made in (14) that only inward traveling waves leave the boundary. When $\partial\mathbb{D}$ is irregular (which is the case when the sources are randomly distributed) these cross products do not integrate coherently and hence the spurious events are suppressed [7]. Since the medium at and outside $\partial\mathbb{D}$ is homogeneous and isotropic, the spurious events are absent when both $\boldsymbol{x}_A$ and $\boldsymbol{x}_B$ are located inside $\mathbb{D}$.

1) Transient Sources: Expressions for transient can be obtained for correlation-type interferometry. We define the matrix of measured electric fields generated by transient electric current sources as

$$\hat{\mathcal{E}}^{\text{obs}}(\boldsymbol{x}_{A,B}, \boldsymbol{x}, \omega) = \hat{\boldsymbol{G}}^{Ee}(\boldsymbol{x}_{A,B}, \boldsymbol{x}, \omega)\hat{\boldsymbol{S}}(\boldsymbol{x}, \omega) \quad (16)$$

where $\hat{\boldsymbol{S}}(\boldsymbol{x}, \omega) = \text{diag}[s_1(\boldsymbol{x}, \omega), s_2(\boldsymbol{x}, \omega), s_3(\boldsymbol{x}, \omega)]$ denotes the source spectrum matrix at position $\boldsymbol{x}$, which can be different for each direction and for each source position. The power spectrum matrix of the sources is defined as

$$\hat{\boldsymbol{S}}^P(\boldsymbol{x}, \omega) = \text{diag}\left(|s_1(\boldsymbol{x}, \omega)|^2, |s_2(\boldsymbol{x}, \omega)|^2, |s_3(\boldsymbol{x}, \omega)|^2\right). \quad (17)$$

Using these definitions in (15), we find

$$\hat{\boldsymbol{G}}^{Ee}(\boldsymbol{x}_B, \boldsymbol{x}_A, \omega)\chi_{\mathbb{D}}(\boldsymbol{x}_A) + \left\{\hat{\boldsymbol{G}}^{Ee}(\boldsymbol{x}_B, \boldsymbol{x}_A, \omega)\right\}^* \chi_{\mathbb{D}}(\boldsymbol{x}_B)$$
$$\approx -\frac{2}{c\mu}\int_{\boldsymbol{x}\in\partial\mathbb{D}} \hat{\mathcal{E}}^{\text{obs}}(\boldsymbol{x}_B, \boldsymbol{x}, \omega)(\hat{\boldsymbol{S}}^P)^{-1}\left\{\hat{\mathcal{E}}^{\text{obs}}(\boldsymbol{x}_A, \boldsymbol{x}, \omega)\right\}^\dagger d^2\boldsymbol{x}$$

$$(18)$$

where the approximate sign has replaced the equality sign because we have omitted the explicit mention of the "ghost" term. The fact that the inverse of the power spectrum matrix is required indicates that it should be known to use this method for transient sources.

2) Uncorrelated Noise Sources: For mutually uncorrelated noise sources, we require that the sources obey the following relation $\langle\hat{n}(\boldsymbol{x}, \omega)\hat{n}^\dagger(\boldsymbol{x}', \omega)\rangle = 2Y\hat{S}(\omega)\boldsymbol{I}\delta(\boldsymbol{x} - \boldsymbol{x}'), Y = 1/(c\mu)$ being the plane wave admittance. The electric field vector at an observation point is then defined as

$$\hat{\boldsymbol{E}}^{\text{obs}}(\boldsymbol{x}_{A,B}, \omega) = \int_{\boldsymbol{x}\in\partial\mathbb{D}} \hat{\boldsymbol{G}}^{Ee}(\boldsymbol{x}_{A,B}, \boldsymbol{x}, \omega)\hat{n}(\boldsymbol{x}, \omega)d^2\boldsymbol{x}. \quad (19)$$

If we use these definitions in (15), we obtain

$$\hat{\boldsymbol{G}}^{Ee}(\boldsymbol{x}_B, \boldsymbol{x}_A, \omega)\hat{S}(\omega)\chi_{\mathbb{D}}(\boldsymbol{x}_A)$$
$$+ \left\{\hat{\boldsymbol{G}}^{Ee}(\boldsymbol{x}_B, \boldsymbol{x}_A, \omega)\right\}^* \hat{S}(\omega)\chi_{\mathbb{D}}(\boldsymbol{x}_B)$$
$$\approx -\left\langle\hat{\boldsymbol{E}}^{\text{obs}}(\boldsymbol{x}_B, \omega)\left\{\hat{\boldsymbol{E}}^{\text{obs}}(\boldsymbol{x}_A, \omega)\right\}^\dagger\right\rangle. \quad (20)$$

From (20), it is clear that no integration over the source coordinates along the boundary surface is necessary. The presence of the power spectrum $\hat{S}$ indicates that the retrieved Green's function is weighted with the square of the amplitude spectrum of the noise source and a band limited amplitude will result in a smaller effective bandwidth in the final result. The time-domain equivalent is given by

$$\int_{t'=-\infty}^{\infty} \boldsymbol{G}^{Ee}(\boldsymbol{x}_B, \boldsymbol{x}_A, t')S(t - t')dt'\chi_{\mathbb{D}}(\boldsymbol{x}_A)$$
$$+ \int_{t'=-\infty}^{\infty} \boldsymbol{G}^{Ee}(\boldsymbol{x}_B, \boldsymbol{x}_A, -t')S(t - t')dt'\chi_{\mathbb{D}}(\boldsymbol{x}_B)$$
$$\approx -\left\langle\int_{t'=-\infty}^{\infty} \boldsymbol{E}^{\text{obs}}(\boldsymbol{x}_B, t + t')\left\{\boldsymbol{E}^{\text{obs}}(\boldsymbol{x}_A, t')\right\}^{\text{T}} dt'\right\rangle$$

$$(21)$$

and expresses that the cross correlation of electric field measurements at two locations yields the electric field Green's function and its time-reversed counterpart between those two locations convolved with the autocorrelation of the noise sources.

B. Convolution-Type Interferometry

Applying the same analysis, as used for the derivation of (13) and (15), (12) leads to

$$
\hat{\boldsymbol{G}}^{Ee}(\boldsymbol{x}_B, \boldsymbol{x}_A, \omega)\left[\chi_{\mathbb{D}}(\boldsymbol{x}_A) - \chi_{\mathbb{D}}(\boldsymbol{x}_B)\right]
$$
$$
= \frac{1}{j\omega\mu} \oint_{\partial\mathbb{D}} \hat{\boldsymbol{G}}^{Ee}(\boldsymbol{x}_B, \boldsymbol{x}, \omega)
$$
$$
\times \left\{\boldsymbol{n}\cdot\nabla\hat{\boldsymbol{G}}^{Ee}(\boldsymbol{x}_A, \boldsymbol{x}, \omega)\right\}^{\mathrm{T}} d^2\boldsymbol{x}
$$
$$
- \frac{1}{j\omega\mu} \oint_{\partial\mathbb{D}} \left\{\boldsymbol{n}\cdot\nabla\hat{\boldsymbol{G}}^{Ee}(\boldsymbol{x}_B, \boldsymbol{x}, \omega)\right\}\left\{\hat{\boldsymbol{G}}^{Ee}(\boldsymbol{x}_A, \boldsymbol{x}, \omega)\right\}^{\mathrm{T}} d^2\boldsymbol{x}
$$
$$
\tag{22}
$$

and in the far-field approximation, we have

$$
\hat{\boldsymbol{G}}^{Ee}(\boldsymbol{x}_B, \boldsymbol{x}_A, \omega)\left[\chi_{\mathbb{D}}(\boldsymbol{x}_A) - \chi_{\mathbb{D}}(\boldsymbol{x}_B)\right] + \text{``ghost''}
$$
$$
= -\frac{2}{c\mu} \oint_{\partial\mathbb{D}} \hat{\boldsymbol{G}}^{Ee}(\boldsymbol{x}_B, \boldsymbol{x}, \omega)\left\{\hat{\boldsymbol{G}}^{Ee}(\boldsymbol{x}_A, \boldsymbol{x}, \omega)\right\}^{\mathrm{T}} d^2\boldsymbol{x}. \tag{23}
$$

For convolution-type interferometry only transient sources can be used. Using the same definition of the transient source matrix and the observed electric field matrix, we obtain

$$
\hat{\boldsymbol{G}}^{Ee}(\boldsymbol{x}_B, \boldsymbol{x}_A, \omega)\left[\chi_{\mathbb{D}}(\boldsymbol{x}_A) - \chi_{\mathbb{D}}(\boldsymbol{x}_B)\right]
$$
$$
\approx -\frac{2}{c\mu} \int_{\boldsymbol{x}\in\partial\mathbb{D}} \hat{\mathcal{E}}^{\mathrm{obs}}(\boldsymbol{x}_B, \boldsymbol{x}, \omega)(\hat{\boldsymbol{S}}^2)^{-1}\left\{\hat{\mathcal{E}}^{\mathrm{obs}}(\boldsymbol{x}_A, \boldsymbol{x}, \omega)\right\}^{\mathrm{T}} d^2\boldsymbol{x}
$$
$$
\tag{24}
$$

where it is noted that $\hat{\boldsymbol{S}}^2$ is the square of complex source spectra, given by $\hat{\boldsymbol{S}}^2(\boldsymbol{x}, \omega) = \mathrm{diag}(s_1^2(\boldsymbol{x}, \omega), s_2^2(\boldsymbol{x}, \omega), s_3^2(\boldsymbol{x}, \omega))$, and hence the cross-convolution method is not suitable for uncorrelated noise sources. In the next section, it is shown that the approximate sign of (24) represents the "ghost" term of (23), which occur as spurious events that are suppressed when the boundary is irregular.

VI. EXAMPLES

Here, we work out a 2-D example for GPR. In the usual GPR acquisition configuration, we use two parallel broadside antennas which reduce to a TE-mode acquisition set up in a 2-D setting. We assume that there are several TE-mode line sources of EM fields in the air and below the bottom interface, and that these sources lie on a straight line (see Fig. 1). One observation point is located just above the surface and the other is in the air above the top boundary. Below the surface a two-layered half-plane is considered, each layer being homogeneous. The examples we show come from this three-layered model, upper half-space is air and modeled as free space, the second layer has a thickness of 1 m and the relative electric permittivity is $\varepsilon_r = 9$, while the relative electric permittivity of the lower half-space is $\varepsilon_r = 16$. The upper source level, $x_{3;1}$ is 2-m above the surface where the antennas are placed, while the lower source level, $x_{3;2}$, is 2 m below the bottom surface in the lower half-
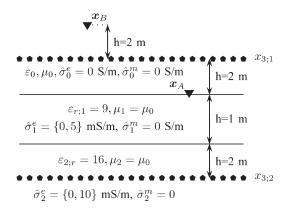

Fig. 1. Configuration for the 2-D examples, with a three-layer medium and with zero and nonzero values for the electric conductivity to investigate the effects of conductivity in cross-correlation interferometry methods.

space. The sources are separated by 10 cm in the horizontal direction and we have used 151 sources spanning a horizontal offset of 7.5 m in both directions. The source time signature of each boundary source is a second derivative of a Gaussian with a 250-MHz center frequency.

A. Correlation Gathers

One antenna is located in air above the top boundary and the causal Green's function is retrieved. The contribution from the separate sources at the top boundary and at the bottom boundary are given in Fig. 2. These results are obtained with (13). Contributions from each surface have noncausal events, labeled nc_1 and nc_2, that are canceled when they are summed to obtain the final result. It can be observed in Fig. 2(a) and (c) that the direct event, event number one, from the top surface has the wrong sign and corrects the event from the bottom surface, whose amplitude is too large. The direct wave is mostly constructed from contributions of sources at the bottom surface, while the sources at both surfaces contribute equally to the reflection event, event number two. When the far-field approximation of (18) is used, the sign of the noncausal events is reversed to favor inward traveling waves from the top surface and hence nonphysical events are introduced, as is shown in Fig. 3, labeled s_1, s_2. It can be seen in the figure that new "ghost" events show up, labeled s_3 to s_6, which remain in the final result. These are due to incomplete destructive interference because we have assumed that the generalized rays that leave the surface in the $\pm x_3$-direction give the major contribution. This assumption is clearly violated by the contribution from sources at the top boundary. All nonphysical events are coming from sources at the top boundary and arise at negative times, or at least before the first physical arrival, because they come from correlations of waves that travel from the boundary outward to $\boldsymbol{x}_B$ and inward from the boundary to $\boldsymbol{x}_A$, whose travel time is larger than the travel time to $\boldsymbol{x}_B$ from which is subtracted. The effect of the far-field approximation is small and limited to a decrease in recovered amplitude of the direct arrival, as shown in the figure, where the exact interferometric result is plotted together with the result obtained with the far-field approximation. Equations (18) and (20) are suitable for interferometric applications because all artifacts occur outside the time window of interest and can be identified.
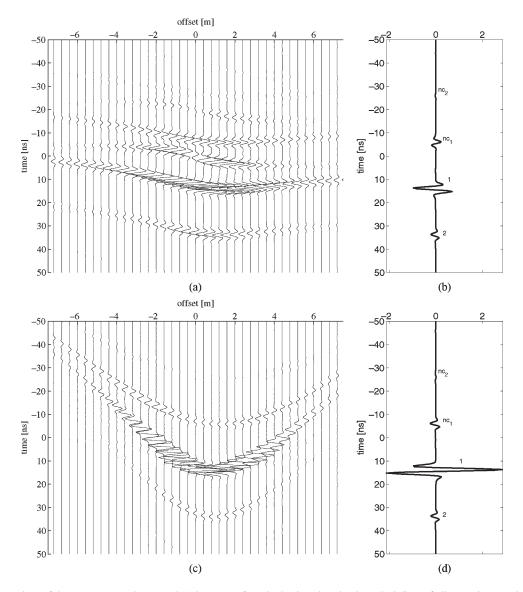
Fig. 2.   Correlation gathers of the sources at (a) the top and (c) bottom surfaces in the time domain. (b) and (d) Sum of all traces in (a) and (c) at the amplitude scale of the exact result.

Moreover, the "ghost" events all occur in a time-symmetric manner relative to a common arrival time at zero horizontal source–receiver offset. This is illustrated in Fig. 4, where a common-midpoint gather is shown of the total result from both surfaces obtained using (18). It can be observed that s_1, s_3, s_2, s_4 and s_5, s_6 form time-symmetric pairs. Under favorable conditions, this allows cleaning up the data by successive mirroring and subtracting these events from the data. This is only necessary when large horizontal offsets are used because then the earliest "ghost" event overlaps the direct arrival.

B. Effect of Conduction Losses in Correlation Results

The configurations described in this paper allow correlation-type interferometry only for zero conductivity and relaxation mechanisms, while the convolution-type interferometry is valid in conductive media. We show in Fig. 5 one example of the effects of nonzero conductivity values on correlation results for x_B in the air above the top surface. It is first observed that the contributions from the bottom boundary have almost vanished.

This is because the waves must travel 2 m from this surface to the deepest interface in the target zone and the energy that is lost along this path cannot be recovered. A second observation is that in the contributions from the top surface no new "ghost" events occur relative to the ones present in the equivalent but lossless case, compare with Fig. 3. The direct arrival in the final result has the wrong sign, as expected from the top boundary result that was also seen in the lossless case, but the first primary reflection, labeled event number 2, is almost correctly retrieved. From this result, we conclude that (18) and (20) are suitable for interferometric imaging applications in weakly dissipative media because all artifacts occur outside the time window of interest and can be identified, and the kinematics of all events are correct.

C. Convolution Gathers

The configuration shown above in correlation gathers is also suitable for convolution-type interferometry. In this configu-ration, the bottom boundary has exactly a zero contribution
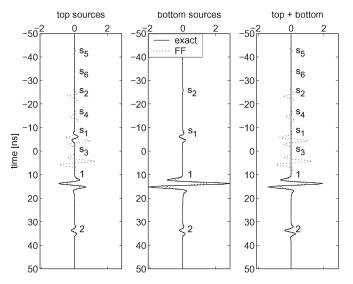
Fig. 3. Comparison of the exact interferometric results and results from the far-field approximation in the separate contributions from sources at the top surface (left), bottom surface (middle), and their total sum (right).
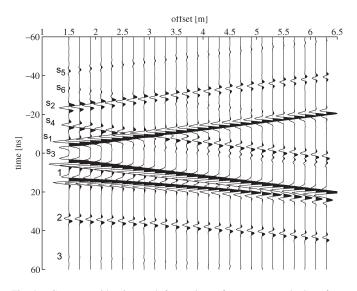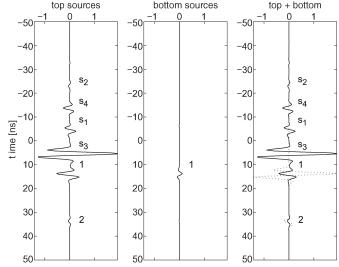

Fig. 5. Results from the far-field approximation of (18) in conductive media. The left and middle graphs show the separate contributions from sources at the top surface and bottom surface, respectively. The total sum (solid line) is compared to the forward-modeled response (dotted line) in the right graph.

Fig. 4. Common mid-point result for total sum from sources at both surfaces and using the far-field approximation.

and only the top surface needs to be considered, because the contribution from the bottom surface vanishes. This can be understood from the observation that when we keep the boundary and the two receiver locations fixed, the total contribution is fixed. By moving the top boundary to positions that both receiver locations are inside $\mathbb{D}$, the total result is always zero independent of the location of the bottom boundary and hence the bottom boundary has a vanishing contribution. This implies that while downgoing waves leaving the domain $\mathbb{D}$ are not recorded, the upgoing waves must cancel. The integrand in (22) shown in the time domain for all the separate sources form the convolution gather and the left-hand side of (18) in the time-domain forms a single trace. Both are shown in Fig. 6. In the figure, it can be seen that the contribution from the stationary point is the earliest event in time of the convolution gather response curve. This is because now arrival times are added and the shortest path yields the physical event. It can also be

observed that the amplitudes of arrivals further away from the stationary point drop faster than the corresponding curves in the correlation gather. A third observation is that in between the arrivals of the physical events, there are curved events that sum up to zero. Since now, arrival times are added, using the far-field approximation yields "ghost" events, whose arrival times are inherently positive and occur in the time window of interest. These "ghost" events have information about the location of the sources on the boundary surface and when this surface is irregular, the "ghost" events will be suppressed by destructive interference as shown by Draganov *et al.* [7] for correlation-type interferometry. We show here in Fig. 7 that when (24) is used, similar events are present in the convolution results in the time window of interest in (a), where the dotted curve has one spurious event in the time window between 20 and 30 ns, and that it is suppressed by taking irregularly spaced source heights to define the top boundary, as shown in (b), where we have defined the top boundary by 100 random values in the range of ± 50 cm relative to the mean height of 2 m. Some small amplitudes of the "ghost" events remain in the time window from 20 to 30 ns. Further reduction of the spurious events can be obtained by introducing more heights. Still, the physical events are all correctly retrieved, even in this situation with nonzero conductivity values in the layers below the surface. We therefore conclude that the cross-convolution method applied on data from transient sources in dissipative media is the most accurate interferometric method when the boundary is sufficiently irregular, because all physical events are retrieved correctly.

VII. CONCLUSION

We have formulated exact Green's function representations for EM fields and waves between two points in terms of cross correlations and cross convolutions of recordings at those two points. Necessary modifications are presented for applications in GPR interferometry. This is possible in a configuration
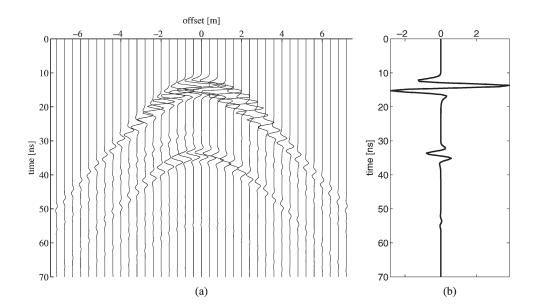
Fig. 6.   Convolution gather of the sources at (a) the top surface in the time domain. (b) Shows the sum of all traces in (a) at its own exact amplitude scale.

where the medium outside the domain $\mathbb{D}$ is homogeneous. In the configuration where one observation point is outside the domain spanned by the sources, outward traveling waves always interact with inward traveling waves and spurious events occur. In cross-correlation-type interferometry, these spurious events occur before the first physical event and can be easily identified. The physical events are retrieved correctly in lossless media, while in dissipative media amplitude errors occur, but no new spurious events arise. In cross-convolution-type interferometry these "ghost" events inherently arrive in the time window of interest. For both correlation and convolution-type interferometry, these spurious events are suppressed effectively when the sources lie on an irregular boundary surface. When transient sources can be used, the cross-convolution method is the preferred method for Green's function retrieval in lossy media. An example can be the extension of crosshole GPR tomography. When three boreholes are in a line and the distance between the outer most boreholes is too large for direct measurement between the holes, this data can be obtained using cross convolutions of data recorded simultaneously in both holes from sources in the center hole. For most GPR applications, where the dissipation is not too strong and noise sources must be used, the cross-correlation method can be used.

The advantage of interferometric methods is that naturally present ambient noise can be used as the source, allowing for all kinds of GPR without a source applications. Low-quality recordings can be made, because correlation and convolution processes enhance the signal-to-noise ratio. Contributions from many sources are added for many time samples to reconstruct a single time sample for a new data trace (A-scan). An example where 1-bit recordings were successfully used for Green's function retrieval is given in [9]. Scattering from objects enhances the quality of the reconstructions, in fact when the medium is so heterogeneous that the wavefield becomes diffuse, the spurious events are more strongly suppressed, this has been shown in [20], [28], [32], and [33]. If system noise and/or clutter noise is coherent, this noise can lead to amplitude errors and spurious

events, for which reason, we should operate receivers and antennas with a very low noise floor.

After the interferometry process, every receiver has played the role of a new source, so from a recording of N different receiving antennas, N source positions can be synthesized, and for each source N receivers can be used with one autocorrelation and $N-1$ cross correlations. This generates a full multistatic data set. When multicomponent data are recorded, full polarimetric multistatic data can be created. Passive imaging techniques used on ultrawideband data again combines data from these new sources and receivers and further enhances the signal-to-noise ratio. The original sources on the boundary could be either noise or transient sources, which can be unknown or controlled. When these are uncorrelated noise sources, they can emit simultaneously but if they are transient sources, they must emit signals in a form that allows for them to be recorded separately. Examples of such sources are background radiation in a wide frequency band and satellite signals in smaller bands. In the atmosphere there are many sources of EM energy in low-frequency ranges, as well as in the bands used for radio waves and wireless communication. From stationary phase analysis, we know that not all points on the boundary are equally important. The target depth and required survey size for the receivers determines the required horizontal extent of sources on the boundary. A general good estimate would be that the sources are on a boundary that exceeds the receiver array on both sides by at least the target depth range. Then, accurate data can be created for all possible offsets in the interferometric result. With present day emergence of ultrawideband EM components, it will become possible to carry out such experiments. That would open a whole new range of EM applications. For small band signals the first EM experiments are reported by Lerosey *et al.* [10] for time reversal and by Henty and Stancil [8] for superresolution focusing in the frequency domain. Other examples are the decomposition of the time reversal operator method [13], the method of interferometric aperture synthesis radiometry [4] and focusing
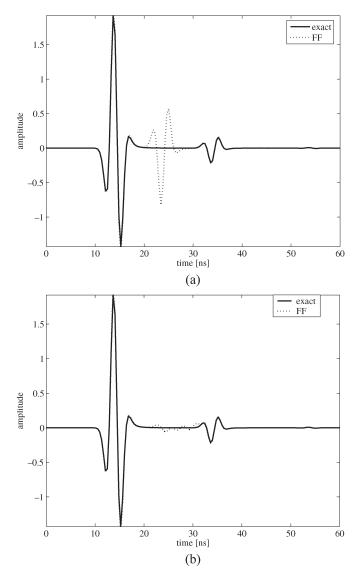
Fig. 7. Comparison of exact result with conductive layers (solid line) and the result with the far-field approximation (dotted line) from sources at the top boundary with (a) a constant height distribution and with (b) an irregular height distribution.

in time-reversed random fields [14]. Since we have formulated representations for lossy media, they can be used for diffusive EM fields and stationary electric currents.

REFERENCES

[1] N. Bojarski, "Generalized reaction principles and reciprocity theorems for the wave equations, and the relationships between time-advanced and time-retarded fields," *J. Acoust. Soc. Amer.*, vol. 74, no. 1, pp. 281–285, Jul. 1983.

[2] M. Campillo and A. Paul, "Long-range correlations in the diffuse seismic coda waves," *Science*, vol. 299, pp. 547–549, 2003.

[3] J. Claerbout, "Synthesis of a layered medium from its acoustic transmission response," *Geophysics*, vol. 33, no. 2, pp. 264–269, Apr. 1968.

[4] I. Corbella, N. Duffo, M. Vall-llossera, A. Camps, and F. Torres, "The visibility function in interferometric aperture synthesis radiometry," *IEEE Trans. Geosci. Remote Sens.*, vol. 42, no. 8, pp. 1677–1682, Aug. 2004.

[5] A. de Hoop, *Handbook of Radiation and Scattering of Waves*. Amsterdam, The Netherlands: Academic Press, 1995.

[6] A. Derode, E. Larose, M. Tanter, J. de Rosny, A. Tourin, M. Campillo, and M. Fink, "Recovering the Green's function from field-field correlations in an open scattering medium (L)," *J. Acoust. Soc. Amer.*, vol. 113, no. 6, pp. 2973–2976, Jun. 2003.

[7] D. Draganov, K. Wapenaar, and J. Thorbecke, "Seismic interferometry: Reconstructing the earth's reflection response," *Geophysics*, vol. 71, no. 4, pp. SI61–SI70, Jul./Aug. 2006.

[8] B. Henty and D. Stancil, "Multipath-enabled super-resolution for rf and microwave communication using phase-conjugate arrays," *Phys. Rev. Lett.*, vol. 93, no. 24, pp. 243 904-1–243 904-4, Dec. 2004.

[9] E. Larose, A. Derode, M. Campillo, and M. Fink, "Imaging from one-bit correlations of wideband diffuse wave fields," *J. Appl. Phys.*, vol. 95, no. 12, pp. 8393–8399, Jun. 2004.

[10] G. Lerosey, J. de Rosny, A. Tourin, A. Derode, G. Montaldo, and M. Fink, "Time reversal of electromagnetic waves," *Phys. Rev. Lett.*, vol. 92, no. 19, pp. 193 904-1–193 904-3, May 2004.

[11] I. Lindell, A. Sihvola, S. Tretyakov, and A. Viitanen, *Electromagnetic Waves and Bi-Isotropic Media*. Boston, MA: Artech House, 1994.

[12] O. Lobkis and R. Weaver, "On the emergence of the Green's function in the correlations of a diffuse field," *J. Acoust. Soc. Amer.*, vol. 110, no. 6, pp. 3011–3017, Dec. 2001.

[13] G. Micolau, M. Saillard, and P. Borderies, "DORT method as applied to ultrawideband signals for detection of buried objects," *IEEE Trans. Geosci. Remote Sens.*, vol. 41, no. 8, pp. 1813–1820, Aug. 2003.

[14] C. Oestges, A. Kim, G. Papanicolaou, and A. Paulraj, "Characterization of space-time focusing in time-reversed random fields," *IEEE Trans. Antennas Propag.*, vol. 53, no. 1, pp. 283–293, Jan. 2005.

[15] P. Roux, K. Sabra, W. Kuperman, and A. Roux, "Ambient noise cross correlation in free space: Theoretical approach," *J. Acoust. Soc. Amer.*, vol. 117, no. 1, pp. 79–84, Jan. 2005.

[16] B. R.-S. Cheo, "A reciprocity theorem for electromagnetic fields with general time dependence," *IEEE Trans. Antennas Propag.*, vol. 13, no. 3, pp. 278–284, Mar. 1965.

[17] N. Shapiro, M. Campillo, L. Stehly, and M. Ritzwoller, "High-resolution surface-wave tomography from ambient seismic noise," *Science*, vol. 307, no. 5715, pp. 1615–1618, Mar. 2005.

[18] E. Slob, D. Draganov, and K. Wapenaar, "GPR without a source," in *Proc. 11th Int. Conf. GPR*, 2006, p. ANT.6.

[19] E. Slob, D. Draganov, and K. Wapenaar, "Let the FCC rules work for you: Turning commercial noise into useful data," in *Proc. 11th Int. Conf. GPR*, 2006, p. AIR.5.

[20] E. Slob and K. Wapenaar, "Electromagnetic Green's functions retrieval by cross-correlation and cross-convolution in media with losses," *Geoph. Res. Lett.*, vol. 34, no. 5, L05307, Mar. 2007.

[21] E. Slob, D. Draganov, and K. Wapenaar, "Interferometric electromagnetic Green's functions representations using propagation invariants," *Geoph. J. Int.*, vol. 169, no. 1, pp. 60–80, Mar. 2007.

[22] R. Snieder, "Extracting the Green's function from the correlation of coda waves: A derivation based on stationary phase," *Phys. Rev. E, Stat. Phys. Plasmas Fluids Relat. Interdiscip. Top.*, vol. 69, no. 4, pp. 046 610-1–046 610-8, Apr. 2004.

[23] R. Snieder, "Retrieving the Green's function of the diffusion equation from the response to a random forcing," *Phys. Rev. E, Stat. Phys. Plasmas Fluids Relat. Interdiscip. Top.*, vol. 74, no. 4, pp. 046 620-1–046 620-4, Oct. 2006.

[24] D.-J. van Manen, A. Curtis, and J. Robertsson, "Interferometric modeling of wave propagation in inhomogeneous elastic media using time reversal and reciprocity," *Geophysics*, vol. 71, no. 4, pp. SI47–SI60, Jul./Aug. 2006.

[25] D.-J. van Manen, J. Robertsson, and A. Curtis, "Modeling of wave propagation in inhomogeneous media," *Phys. Rev. Lett.*, vol. 94, no. 16, pp. 164 301-1–164 301-4, Apr. 2005.

[26] B. van Tiggelen, "Green function retrieval and time reversal in a disordered world," *Phys. Rev. Lett.*, vol. 91, no. 24, pp. 243 904-1–243 904-4, Dec. 2003.

[27] K. Wapenaar, "Retrieving the elastodynamic Green's function of an arbitrary inhomogeneous medium by cross correlation," *Phys. Rev. Lett.*, vol. 93, no. 25, pp. 254 301-1–254 301-4, Dec. 2004.

[28] K. Wapenaar, "Green's function retrieval by cross-correlation in case of one-sided illumination," *Geophys. Res. Lett.*, vol. 33, no. 19, pp. L19 304-1–L19 304-6, Oct. 2006.

[29] K. Wapenaar, D. Draganov, J. Thorbecke, and J. Fokkema, "Theory of acoustic daylight imaging revisited," in *Proc. Expanded Abstracts 72nd Annu. Int. Meeting Soc. Expl. Geophys.*, 2002, pp. 2269–2272.

[30] K. Wapenaar and J. Fokkema, "Reciprocity theorems for diffusion, flow and waves," *ASME J. Appl. Mech.*, vol. 71, no. 1, pp. 145–150, Jan. 2004.

[31] K. Wapenaar, E. Slob, and R. Snieder, "Unified Green's function retrieval by cross correlation," *Phys. Rev. Lett.*, vol. 97, no. 23, pp. 234 301-1–234 301-4, Dec. 2006.

[32] R. Weaver and O. Lobkis, "Ultrasonics without a source: Thermal fluctuation correlations at MHz frequencies," *Phys. Rev. Lett.*, vol. 87, no. 13, pp. 134 301-1–134 301-4, Sep. 2001.

[33] R. Weaver and O. Lobkis, "Diffuse fields in open systems and the emergence of the Green's function (L)," *J. Acoust. Soc. Amer.*, vol. 116, no. 5, pp. 2731–2734, Nov. 2004.

Kees Wapenaar received the M.Sc. and Ph.D. degrees in applied physics from the Delft University of Technology, Delft, The Netherlands, in 1981 and 1986, respectively.

From 1986 to 1999, he was an Associate Professor and one of the project leaders of the Delphi consortium (a project on seismic imaging and characterization) at the Faculty of Applied Physics in Delft. In 1999, he was appointed Professor of applied geophysics at the Faculty of Civil Engineering and Geosciences. Since 2002, he has been the Chair in the section of applied geophysics and petrophysics at this faculty, and since 2005, he has been also Scientific Director of the Department of Geotechnology. His main research interests are wave theory and its applications in geophysical imaging and characterization, multicomponent seismics, and passive seismic reflection imaging. He published one book and 90 journal papers on these subjects. As of September 2007, he will serve as Editor-in-chief for *Geophysics*.

Evert Slob received the M.Sc. degree in mining and petroleum engineering and the Ph.D. degree (*cum laude*) in technical sciences from the Delft University of Technology (TUDelft), Delft, The Netherlands, in 1989 and 1994, respectively.

In 1995, he was with the Department of Geotechnology, TUDelft, where he is currently an Associate Professor in applied geophysics. He serves as GPR and electromagnetic (EM) rock properties Associate Editor for *Geophysics*, and on GPR for *Near Surface Geophysics*. His current research interests are EM fields and wave theory and its applications in geophysical imaging and inversion techniques, both with active and passive sources; heterogeneity determination and soil characterization, including the study of fundamental relations between geological and EM properties, of soil and rocks, and their scale dependence. He published 30 journal papers on these subjects.

Dr. Slob served as the General Chairman of the 10th International Conference on Ground Penetrating Radar (GPR2004), Delft, The Netherlands. He has organized three workshops on GPR and has been Guest Editor of four special issues on GPR.